

TEMPO-Oxidized Cellulose Beads for Cationic Dye Adsorption

Qianqian Wang,^{a,b,c,*} Simeng Liu,^b Honglei Chen,^{a,*} Jun Liu,^b and Qianqian Zhu^{a,b}

Toxic organic dyes present in wastewater should be removed before discharge. In this study, TEMPO-oxidized, regenerated cellulose beads were prepared using a simple falling ball technique for cationic methylene blue (MB) removal. The obtained cellulose beads were characterized using various analytical techniques. The results indicated that TEMPO-oxidized cellulose beads displayed porous structures with high content of carboxylic acid groups. Thus, the negatively charged cellulose beads can effectively adsorb cationic MB with an adsorption capacity of 495 mg/g at a starting concentration of 100 mg/L. This simple one-step adsorption process achieved near-complete MB removal at pH 7, indicating strong electrostatic interactions between cationic MB and negatively charged oxidized cellulose beads. The experimental data can be well described by the Langmuir isotherm model and the Pseudo-second-order model. The fabricated cellulose beads exhibit great potential for practical application in dye removal from wastewater.

DOI: 10.15376/biores.17.4.6056-6066

Keywords: TEMPO oxidation; NaOH/urea solvent; Cellulose beads; Cationic dye; Adsorption

Contact information: a: State Key Laboratory of Bio-based Materials and Green Papermaking, Qilu University of Technology, Jinan 250353, China; b: Biofuels Institute, Jiangsu University, Zhenjiang 212013 China; c: Jinan Shengquan Group Share Holding Co., Ltd., Jinan 250204 China;

* Corresponding authors: qianqian.wz@gmail.com; chenhonglei_1982@163.com

INTRODUCTION

With the rapid development of modern society, surface water quality has deteriorated significantly over the past two to three decades due to human activities and industrial processes (Bolisetty *et al.* 2019; Wang *et al.* 2022a). Water pollutants, such as synthetic dyes, microplastics, pesticides, and metal ions, are widespread in water bodies (Sharma *et al.* 2020; Das *et al.* 2022). Considering these ever-growing pollutants, the development of green- and low-cost water treatment technologies is urgently needed. There are many water purification technologies, such as adsorption, coagulation, membrane filtration, chlorine disinfection, ozonation, and biological treatment. Adsorption-based purification techniques are attractive due to their high efficiency and low cost. Adsorption is effective to remove dyes to minimal concentrations. The high efficiency of this level can be achieved with various adsorbents, such as activated carbons, silica gel, and resins. It is of great significance to develop low-cost adsorbents from renewable and sustainable source materials.

Because cellulose is the most abundant biopolymer in nature, cellulose materials have been extensively examined for versatile applications, as they possess qualities such as sustainability, biodegradability, renewability, low cost, and high availability (Zhu *et al.* 2020a,b,c; Wang *et al.* 2022b). Cellulose adsorbents have also gained increased attention

over the past three decades (Rodrigues *et al.* 2019; Varghese *et al.* 2019; Köse *et al.* 2020a). The insolubility of cellulose has become an advantage but also a bottleneck for its application. Being insoluble and stable in water, the cellulose adsorbents can easily be separated from wastewater streams and can be easily regenerated after pollutant removal (De Luca *et al.* 2003). In contrast, the adsorption capacity of pristine insoluble cellulose is minimal due to the limited adsorption sites. Chemically modified cellulose adsorbents with enhanced adsorption efficiency and physical stability in the form of aerogels, foams, beads, or membranes with large surface area and adsorption capacity have been demonstrated to enable large-scale operation (Gericke *et al.* 2013; Hokkanen *et al.* 2016; Mahfoudhi and Boufi 2017). Versatile synthetic routes for nanostructured cellulose hydrogels and aerogels have been developed in efficient manners (Gericke *et al.* 2013). For example, cellulose beads with great adsorption capacities have been synthesized in cellulose solvents (Pang *et al.* 2016). Preparation and modification techniques for cellulose adsorbents intended for dye removal have been systemically summarized in several great reviews (Mudhoo *et al.* 2019; Batmaz *et al.* 2014). Previous reports indicated that 2,2,6,6-tetramethylpiperidine-1-oxyl (TEMPO-) mediated oxidization of nanocellulose has high affinities and adsorption capacities for metal ions due to the introduction of carboxylic acid groups (Köse *et al.* 2020b). Fe (II) adsorption capacity increased from 23 to 400 mg/g polymer with the implementation of TEMPO-oxidized CNF. Sodium hydroxide-urea (NaOH/urea) solvent system as a low-cost and effective cellulose solvent has attracted great attention (Wang *et al.* 2016). Research on cellulose-derived beads from new solvent systems has received increasing interest.

In this work, cotton linter cellulose was pretreated by TEMPO-mediated oxidation to introduce carboxylic acid groups and was subsequently dissolved in NaOH/urea solvent to synthesize cellulose beads using the falling ball technique. The novelty of this study lies in the fabrication and characterization of TEMPO-oxidized cellulose beads via a combination of TEMPO-oxidization, NaOH/urea dissolution, and falling ball technique. The present study attempts to examine the adsorption behaviors of negatively charged cellulose beads for cationic dye adsorption. Meanwhile, the adsorption isotherm and kinetic models were also examined.

EXPERIMENTAL

Materials

Cotton linter with a viscosity-average molecular weight of 1.07×10^5 g/mol was bought from Hubei Chemical Fiber Group Co., Ltd. (Xiangfan, China). Sodium hydroxide, sodium bromide, urea, hydrochloric acid, ethanol, 2,2,6,6-tetramethylpiperidine-1-oxyl radical (TEMPO), and sodium hypochlorite (10% active chlorine) were purchased from Sinopharm Group Chemical Reagent Co., Ltd. (Shanghai, China).

TEMPO Oxidation of Cotton Linter

Cotton linter was ball-milled to pass through a 40-mesh screen. The TEMPO oxidation was performed according to the previous protocol (Isobe *et al.* 2013). Briefly, 10 g cotton linter powder was suspended in 1.0 L ultrapure water containing 160 mg TEMPO and 1.0 g NaBr. The suspension was stirred continuously at room temperature and then 75 mL NaClO solution was added dropwise over 1, 3, 6, and 12 h with pH maintained at 10 to 10.5. The reaction was quenched with ethanol and the final pH was adjusted to 7.0.

NaOH/urea Dissolution and Cellulose Beads Fabrication

NaOH/urea solvent was used to prepare cellulose beads with porous structures. Approximately 3.5 g of TEMPO-oxidized cellulose was dissolved in 98 g NaOH-urea-H₂O (7:12:81 in weight ratio) solution precooled at -12 °C. A transparent and viscous cellulose solution was obtained after vigorous stirring. Cellulose beads were then fabricated using the falling-ball method (De Wever *et al.* 2022). Specifically, drops of the cellulose solutions from a 5 mL syringe fell into a 2N HCl regeneration bath under magnetic stirring. The distance between the syringe tip and the bath surface was kept at 1.0 cm. The cellulose beads obtained with different pretreatment times were thoroughly washed with DI water and recorded as CB, TCB-1h, TCB-3h, TCB-6h, and TCB-12h.

Characterization of Cellulose Beads

The solid content of cellulose beads was gravimetrically determined before and after freeze-drying. The swelling ratio was gravimetrically determined by immersing the dried cellulose beads in water at 25 °C. Carboxylic acid content was determined by conductometric titration with 0.1 mol NaOH solution. The surface morphology of cellulose beads was imaged with a JSM-7800F scanning electron microscope (SEM) (JEOL, Tokyo, Japan) at 20 kV. Thermogravimetric analysis (TGA) was conducted with a Perkin Elmer TGA 4000 instrument (Waltham, MA, USA) in the range of 30 to 800 °C at a heating rate of 20 °C/min under a nitrogen atmosphere. Fourier transform infrared (FTIR) in transmission was recorded with a Thermo Nicolet Nexus 470 FTIR spectrometer (Waltham, MA, USA). X-ray diffraction (XRD) patterns were acquired using a Bruker D8 Advance diffractometer (Billerica, MA, USA) with Cu K α radiation. The Brunauer-Emmet-Teller (BET) surface area was obtained using a Micromeritics TriStar II automated system (Norcross, GA, USA).

Methylene Blue Adsorption Evaluation

To explore the adsorption capacity of TEMPO-oxidized cellulose beads, cationic methylene blue (MB) was selected as a model compound. For each experiment, 10 mg (dry weight) cellulose beads were added to a conical flask filled with 50 mL MB (50-250 mg/L) solution and then shaken at 160 rpm from 25 to 45 °C. Aqueous samples were taken at time intervals ranging from 0 to 360 min until equilibrium was reached. The MB concentration was quantitatively determined at 662 nm. The amount of MB adsorbed onto cellulose beads was determined as the difference between the total amount of MB initially applied and the amount of free MB in the solution. The equilibrium adsorption was confirmed by no change in various absorbance measurements during adsorption. Adsorption capacity at equilibrium, q_e , was calculated using Eq. 1. The isotherm adsorption data were fitted to the Langmuir isotherm model (Eq. 2) and Freundlich isotherm model (Eq. 3) (Hamidon *et al.* 2022). The kinetic data were fitted to the pseudo-first-order model (Eq. 4) and pseudo-second-order model (Eq. 5) (Hubbe *et al.* 2019).

$$\text{Equilibrium adsorption capacity} \quad q_e = \frac{(c_0 - c_e)}{m} \cdot V \quad (1)$$

$$\text{Langmuir isotherm model} \quad \frac{c_e}{q_e} = \frac{1}{Q_0 \cdot K} + \frac{c_e}{Q_0} \quad (2)$$

$$\text{Freundlich isotherm model} \quad \ln q_e = \ln K_F + \frac{1}{n} \ln c_e \quad (3)$$

$$\text{Pseudo-first-order kinetics} \quad \ln(q_e - q_t) = \ln q_e - K_1 \cdot t \quad (4)$$

$$\text{Pseudo-second-order kinetics} \quad \frac{t}{q_t} = \frac{1}{K_2 \cdot q_e^2} + \frac{t}{q_e} \quad (5)$$

where c_0 and c_e are the initial and equilibrium concentrations (mg/L) of MB; q_t and q_e are the adsorption capacities (mg/g) at time t (min) and equilibrium; Q_0 is the maximum adsorption amount (mg/g); K , K_1 , and K_2 are the Langmuir constant (L mol^{-1}), pseudo-first-order rate constant (min^{-1}), and pseudo-second-order rate constant ($\text{g} \cdot \text{mg}^{-1} \cdot \text{min}^{-1}$), respectively; K_f and n are the Freundlich isotherm constant and exponent, respectively; V is the volume of MB solution (50 mL), and m is the dry weight of cellulose beads (10 mg).

RESULTS AND DISCUSSION

Properties of TEMPO Oxidized Cellulose Beads

The TEMPO-oxidized cotton linter was rapidly dissolved in precooled NaOH/urea aqueous solvent at -12°C . A clear, homogeneous, and viscous cellulose solution was obtained. The TEMPO pretreatment accelerated cellulose dissolution as compared with untreated cellulose. This result can be attributed to the introduction of the carboxylic acid group and the disruption of order regions during TEMPO oxidation. It should be noted that TEMPO-oxidized and NaOH/urea regeneration may increase costs and create new pollutants.

Cellulose solutions prepared under various oxidation times were added dropwise to 2 N HCl solution as an antisolvent. Cellulose beads were formed as HCl rapidly neutralized NaOH. Figure 1 displays the hydrogel beads and SEM images of their surface after freeze-drying. Cellulose drops formed similar spheres with diameters around 3.5 mm. The surface SEM images of these exhibited noticeable differences. Cellulose beads without TEMPO oxidation exhibited a dense and nonporous structure entangled with microfibrils, whereas the surface of cellulose beads after TEMPO oxidation possessed many internal cavities, creating porous networks. Large pores can be found over several hundred nanometers.

Table 1 shows the basic properties of cellulose beads with/without TEMPO pretreatment. The porous beads with pretreatment displayed a low solid content (4.6% to 5.0%) compared to the untreated beads (5.7%). The carboxyl content of native cellulose fibers was 0.027 mmol/g. The carboxyl content increased up to 1.998 mmol/g during the oxidation lasting from 1 to 12 h. The unmodified cellulose beads had a BET surface area of $20.6 \text{ m}^2/\text{g}$, while the surface area improved to $105.8 \text{ m}^2/\text{g}$ when oxidation time was 12 h. This higher surface area was attributed to a high carboxyl content, leading to a more porous gel structure. All cellulose beads exhibited similar average pore sizes in the range of 4.0 to 4.5 nm. As expected, the swelling ratio for cellulose beads increases steadily with the increase of TEMPO oxidation time.

Table 1. Basic Properties of Cellulose Beads with/without TEMPO Oxidation

Sample ID	Average Diameter (mm)	Solid Content (%)	Carboxyl content (mmol/g)	BET Surface Area (m^2/g)	BET Mean Pore Size (nm)	Swelling Ratio at 150 min (%)
CB	3.42	5.7	0.027	20.58	4.08	70.23
TCB-1h	3.45	4.6	0.653	32.11	4.21	85.64
TCB-3h	3.40	4.5	1.031	46.81	4.58	90.53
TCB-6h	3.44	5.0	1.451	96.82	4.16	92.08
TCB-12h	3.51	4.6	1.998	105.78	4.02	94.91

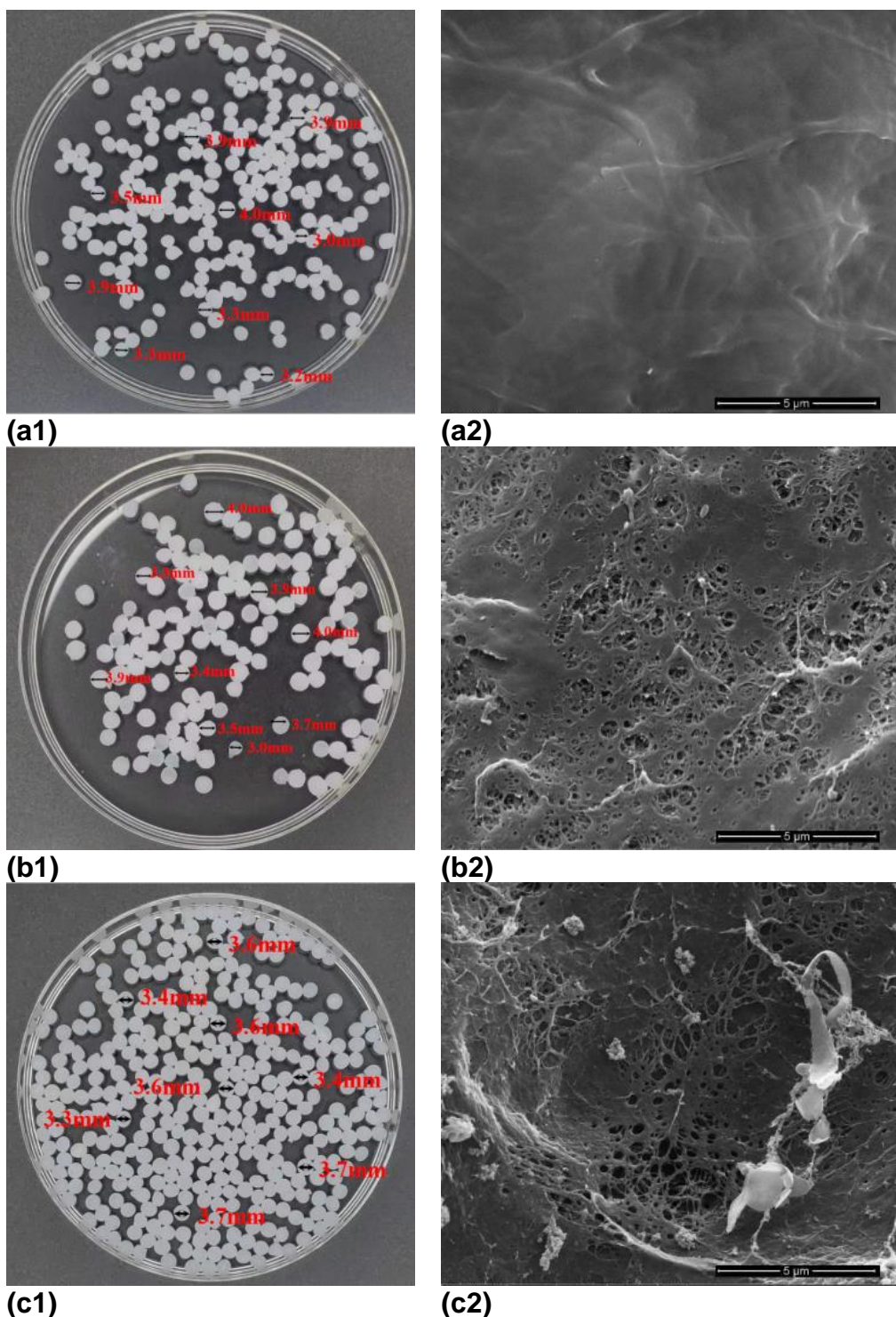


Fig. 1. Digital images of cellulose beads with different oxidation time and their SEM images at surfaces, SEM image scale bar = 5 μm (a: CB; b: TCB-3h; c: TCB-12h)

Thermal stability and infrared spectrum of cellulose beads were examined using TGA and FTIR, respectively (Figs. 2a and 2b). Overall, the cellulose beads prepared with TEMPO oxidation showed slightly declined thermal properties compared to the beads without TEMPO oxidation. All TEMPO-oxidized cellulose beads exhibited similar three-stage degradation trends. The first weight-loss stage was in the temperature range of 25 to

150 °C. This weight loss was less than 10%, corresponding to the removal of moisture as well as adsorbed water. In the second stage, the major weight loss occurred between 150 and 600 °C, which was attributed to the oxidative cleavage of the cellulose chain. Further heating above 600 °C led to the elimination of residual carbon. The FTIR technique can be a straightforward technique to evaluate the structural alterations of cellulose. The FTIR spectrum shows the characteristic peaks of cellulose: -OH stretching at around 3400 cm^{-1} , while the C-H bond stretching vibration was at 2899 cm^{-1} . The narrow peak at 1720 cm^{-1} was due to the ester carbonyl group (C=O) stretching vibration, while the peak for C-H deformation was observed at 896 cm^{-1} (Zhu *et al.* 2020d). Cellulose beads with different carboxylate contents show different peak intensities at 1605 cm^{-1} . However, the carboxylic acid group appeared in very narrow peaks, making quantitative analysis difficult.

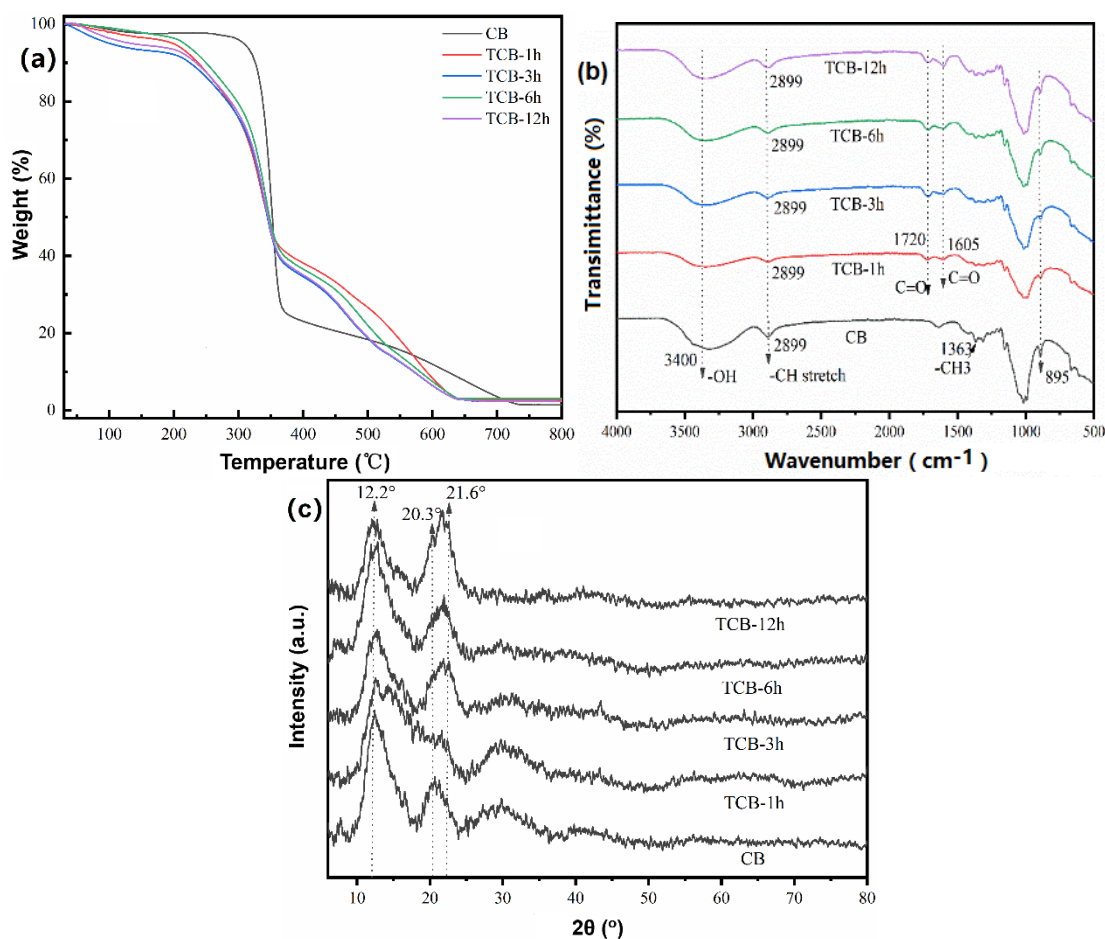


Fig. 2. (a) TGA, (b) FTIR, and (c) XRD of cellulose beads with different oxidation time

In addition to TGA and FTIR, the X-ray analysis of cellulose beads was employed to demonstrate the polymorphic nature of cellulose after dissolution and regeneration. This process transforms cellulose I crystal structure into cellulose II. The XRD patterns of cellulose beads are shown in Fig. 2c. The 12.2° peak can be attributed to the (1-10) reflection of cellulose II at 12°, while the peaks around 20.3° and 21.6° corresponded to the (110) and (020) planes of cellulose II at 20° and 22° 2θ (French 2014; Zhu *et al.* 2020d). The influence of cellulose crystal form transformation on dye adsorption is still unclear, which is worth attention in future research.

Evaluation of MB Adsorption onto Cellulose Beads

Cellulose hydrogel beads with and without TEMPO oxidation were directly used as adsorbents for MB removal from aqueous solutions (100 mg/L). Approximately 10 mg (dry weight) cellulose hydrogel beads were put into 50 mL of MB solution at 25 °C, pH 7, and 160 rpm until equilibrium was reached. The MB removal efficiencies are displayed in Fig. 3a, indicating that the TEMPO oxidation plays an important role. Unoxidized cellulose hydrogel beads removed only 32.5% MB.

The removal extent steadily rose from 79.2% to 99.0% with the increase in carboxyl content. This striking difference can be observed in the digital images as shown in Fig. 3c. The pH has a substantial impact on the adsorption performance of TCB-12h (Fig. 3b). The MB removal efficiency was low at pH 3, 4, and 5 but was quite higher at pH 6. Excess hydrogen ions enter the porous structure of cellulose beads at low pH, protonating the carboxylate groups into uncharged protonated carboxyl groups. The maximum removal efficiency was achieved at neutral pH. The removal efficiency decreased when the pH was higher than 7. The declined adsorption at high pH, for example, 12 is might be attributed to the increased ionic strength.

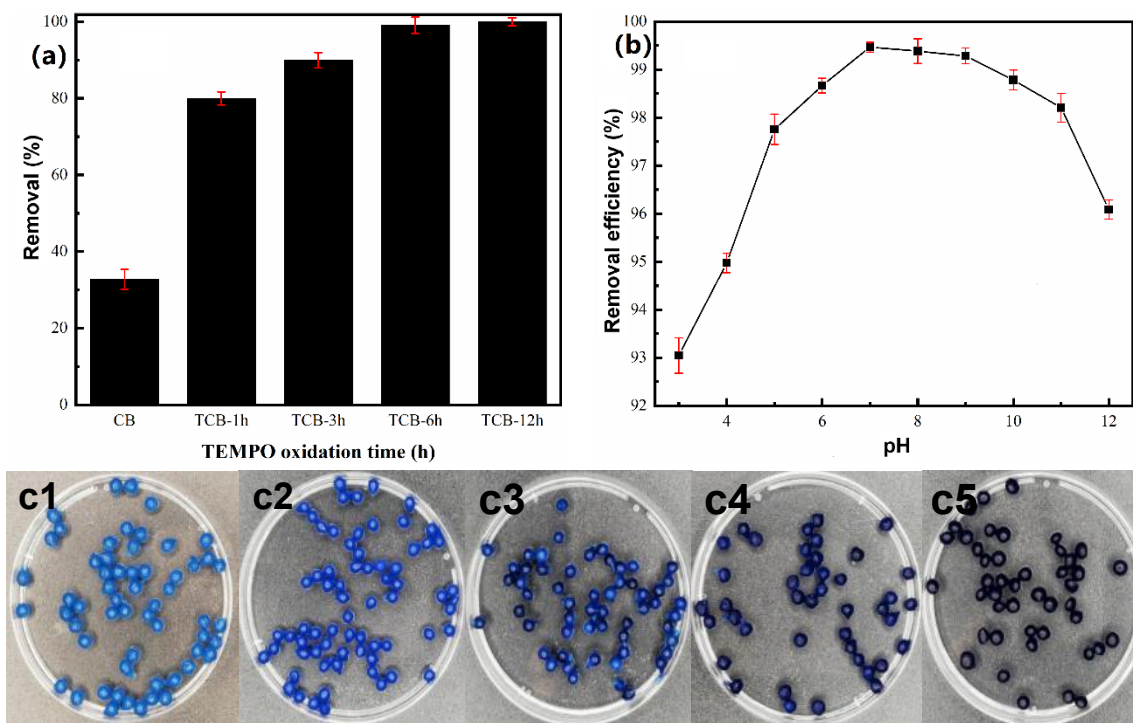


Fig. 3. Effect of oxidation time (a); and pH (b) on MB removal, and digital images (c) of cellulose beads after MB adsorption (c1 CB; c2 TCB-1h; c3 TCB-3h; c4 TCB-6h; c5 TCB-12h)

The isothermal adsorption experiments were conducted with 10 mg TCB-12h cellulose beads at different MB concentrations (50, 100, 150, 200, and 250 mg/L) and temperatures (25, 35, and 45 °C). The most common Langmuir (Eq. 2) and Freundlich (Eq. 3) isotherm models were used to fit the experimental data as shown in Figs. 4a and 4b. Langmuir isotherm model showed a higher value of correlation coefficient ($R^2 > 0.997$) than that of Freundlich isotherm models, indicating monolayer adsorption of MB on homogeneous sites of cellulose beads.

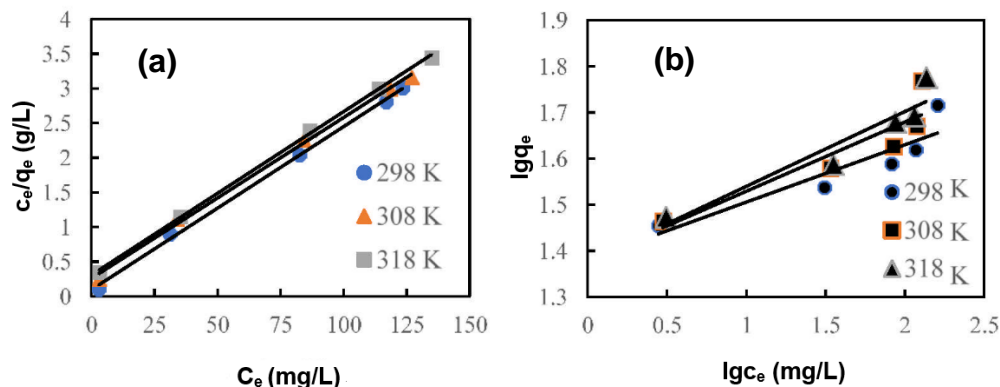


Fig. 4. Langmuir (a) and Freundlich (b) Isotherm modeling of MB adsorption onto cellulose beads (TCB-12h)

The kinetic profiles of adsorption were also characterized during MB adsorption onto TCB-12h cellulose beads. The pseudo-first-order (Eq. 4) and pseudo-second-order (Eq. 5) kinetic models were applied to fit the process as shown in Fig. 5. The kinetic parameters, including the pseudo-first-order rate constant (K_1), pseudo-second-order rate constant (K_2), equilibrium uptake capacity (q_e), and regression coefficient (R^2) were determined. The calculated values are presented in Table 2. It was found that the coefficients of determination for the pseudo-first-order rate constant, K_1 , were higher than that of the pseudo-second-order kinetic values, while the opposite was true for q_e . The R^2 values for the pseudo-second-order kinetics were higher than that of the pseudo-first-order kinetics, indicating that the pseudo-second-order model was more suitable for describing the adsorption kinetics of MB dye onto cellulose beads. Hence, these findings support that the MB dye adsorption rates on cellulose beads strongly depend on both concentration of MB and cellulose beads as well as time. The good fit to the pseudo-second-order rate expression suggests that adsorption was controlled by diffusion into a network of very small pores (Hubbe *et al.* 2019). In this study, the maximum adsorption capacity of TEMPO-oxidized cellulose beads (TCB-12h) reached 495 mg/g. This value is much higher than 48.8 mg/g for porous cellulose microbeads (Hua *et al.* 2019) or 288.8 mg/g for carboxylated cellulose beads (Meng *et al.* 2019), but lower than 873 mg/g for microwave-assisted TEMPO-oxidized cellulose beads (Lin *et al.* 2017). Accordingly, the adsorption capacity may be further enhanced with the fabricated cellulose beads in this study.

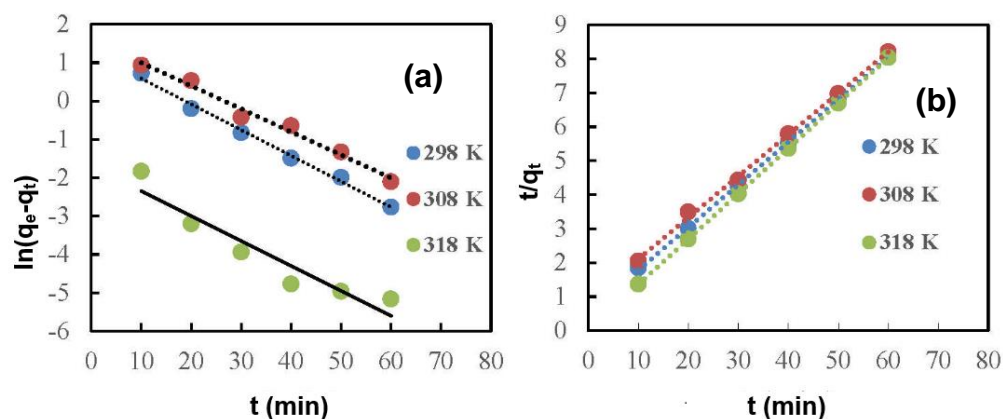


Fig. 5. Pseudo-first-order (a); and pseudo-second-order (b) kinetic modeling for MB adsorption onto cellulose beads (TCB-12h)

Table 2. Fitting Parameters for the Pseudo-first-order and Pseudo-second-order Kinetics

Temperature (K)	Pseudo-first-order Kinetic Model			Pseudo-second-order Kinetic Model		
	K_1 (min^{-1})	q_e ($\text{mg}\cdot\text{g}^{-1}$)	R_1^2	K_2 ($\text{g}\cdot\text{mg}^{-1}\cdot\text{min}^{-1}$)	q_e ($\text{mg}\cdot\text{g}^{-1}$)	R_2^2
98	0.0042	264.67	0.908	8.71193E-05	497.81	0.999
308	0.0045	283.19	0.956	8.33847E-05	498.52	0.999
318	0.0040	234.58	0.802	9.10894E-05	497.33	0.998

CONCLUSIONS

1. Cellulose beads were prepared by the falling ball technique with cotton linter in NaOH/urea solution after TEMPO oxidation. Various amounts of carboxylic acid contents in the range of 0.653 to 1.998 mmol/g were introduced into cellulose beads with average diameters of 3.5 mm. The SEM images indicated that TEMPO-oxidized cellulose beads displayed more pores than untreated cellulose beads.
2. The specific surface area, average pore size, and swelling ratio of cellulose hydrogel microbeads without TEMPO oxidation were 20.58 m^2/g , 4.08 nm, and 70.23%, respectively. After TEMPO oxidation, the maximum specific surface area and swelling ratio of cellulose beads increased to 105.8 m^2/g and 94.9%, respectively, while the average pore size decreased to 4.02 nm.
3. The adsorption capacity of TEMPO-oxidized cellulose beads (TCB-12h) reached 495 mg/g. This facile one-step adsorption process achieved near-complete removal of the MB. The adsorption mechanism followed the Langmuir model and the pseudo-second-order kinetic equation, which indicates that the adsorption rate is controlled by the dye diffusion process into the porous cellulose beads with very narrow pores. Although excellent adsorption capacities were achieved in this study, the cellulose bead fabrication process is still costly and may introduce new pollutants. Thus, it is highly desirable to develop cellulose beads that are environmentally friendly and cost-effective for practical applications.

ACKNOWLEDGMENTS

This work was supported by the State Key Laboratory of Bio-based Materials and Green Papermaking (GZKF202035), Qilu University of Technology, the Jiangsu Province Natural Science Foundation (BK20220552), and the National Natural Science Foundation of China (22278195).

REFERENCES CITED

- Batmaz, R., Mohammed, N., Zaman, M., Minhas, G., Berry, R. M., and Tam, K. C. (2014). "Cellulose nanocrystals as promising adsorbents for the removal of cationic dyes," *Cellulose* 21(3), 1655-1665. DOI: 10.1007/s10570-014-0168-8

- Bolisetty, S., Peydayesh, M., and Mezzenga, R. (2019). "Sustainable technologies for water purification from heavy metals: Review and analysis," *Chemical Society Reviews* 48(2), 463-487. DOI: 10.1039/c8cs00493e
- Das, R., Lindström, T., Sharma, P. R., Chi, K., and Hsiao, B. S. (2022). "Nanocellulose for sustainable water purification," *Chemical Reviews* 122(9), 8936-9031. DOI: 10.1021/acs.chemrev.1c00683
- De Luca, L., Giacomelli, G., Porcheddu, A., Salaris, M., and Taddei, M. (2003). "Cellulose beads: A new versatile solid support for microwave- assisted synthesis. Preparation of pyrazole and isoxazole libraries," *Journal of Combinatorial Chemistry* 5(4), 465-471. DOI: 10.1021/cc0201187
- De Wever, P., Janssens, J., and Fardim, P. (2022). "Fabrication of cellulose cryogel beads via room temperature dissolution in onium hydroxides," *Carbohydrate Polymer Technologies and Applications* 3, article ID 100206. DOI: 10.1016/j.carpta.2022.100206
- French, A. D. (2014). "Idealized powder diffraction patterns for cellulose polymorphs," *Cellulose* 21(2), 885-896. DOI: 10.1007/s10570-013-0030-4
- Gericke, M., Trygg, J., and Fardim, P. (2013). "Functional cellulose beads: Preparation, characterization, and applications," *Chemical Reviews* 113(7), 4812-4836. DOI: 10.1021/cr300242j
- Hamidon, T. S., Adnan, R., Haafiz, M. K. M. and Hussin, M. H. (2022). "Cellulose-based beads for the adsorptive removal of wastewater effluents: A review," *Environmental Chemistry Letters* 20(3), 1965-2017. DOI: 10.1007/s10311-022-01401-4
- Hokkanen, S., Bhatnagar, A., and Sillanpaa, M. (2016). "A review on modification methods to cellulose-based adsorbents to improve adsorption capacity," *Water Research* 91, 156-173. DOI: 10.1016/j.watres.2016.01.008
- Hua, J., Meng, R., Wang, T., Gao, H., Luo, Z., Jin, Y., Liu, L., and Yao, J. (2019). "Highly porous cellulose microbeads and their adsorption for methylene blue," *Fibers and Polymers* 20(4), 794-803. DOI: 10.1007/s12221-019-8334-0
- Hubbe, M. A., Azizian, S., and Douven, S. (2019). "Implications of apparent pseudo-second-order adsorption kinetics onto cellulosic materials: A review," *BioResources* 14(3), 7582-7626. DOI: 10.15376/biores.14.3.7582-7626
- Isobe, N., Chen, X., Kim, U. J., Kimura, S., Wada, M., Saito, T., and Isogai, A. (2013). "Tempo-oxidized cellulose hydrogel as a high-capacity and reusable heavy metal ion adsorbent," *Journal of Hazardous materials* 260, 195-201. DOI: 10.1016/j.jhazmat.2013.05.024
- Köse, K., Mavlan, M., and Youngblood, J. P. (2020a). "Applications and impact of nanocellulose based adsorbents," *Cellulose* 27(6), 2967-2990. DOI: 10.1007/s10570-020-03011-1
- Köse, K., Mavlan, M., Nuruddin, M., and Youngblood, J. P. (2020b). "Tempo-oxidized cellulose nanofiber based polymeric adsorbent for use in iron removal," *Cellulose* 27(8), 4623-4635. DOI: 10.1007/s10570-020-03104-x
- Lin, F., You, Y., Yang, X., Jiang, X., Lu, Q., Wang, T., Huang, B., and Lu, B. (2017). "Microwave-assisted facile synthesis of tempo-oxidized cellulose beads with high adsorption capacity for organic dyes," *Cellulose* 24(11), 5025-5040. DOI: 10.1007/s10570-017-1473-9
- Mahfoudhi, N., and Boufi, S. (2017). "Nanocellulose as a novel nanostructured adsorbent for environmental remediation: A review," *Cellulose* 24(3), 1171-1197. DOI: 10.1007/s10570-017-1194-0

- Meng, R., Liu, L., Jin, Y., Luo, Z., Gao, H., and Yao, J. (2019). "Recyclable carboxylated cellulose beads with tunable pore structure and size for highly efficient dye removal," *Cellulose* 26(17), 8963-8969. DOI: 10.1007/s10570-019-02733-1
- Mudhoo, A., Gautam, R. K., Ncibi, M. C., Zhao, F. P., Garg, V. K., and Sillanpaa, M. (2019). "Green synthesis, activation and functionalization of adsorbents for dye sequestration," *Environmental Chemistry Letters* 17(1), 157-193. DOI: 10.1007/s10311-018-0784-x
- Pang, J. H., Liu, J. K., Zhang, Q. H., Jin, X. J., Zhang, X. M., Yang, J., Xu, F., and Sun, R. C. (2016). "Lightweight and highly adsorptive cellulose beads fabricated in ionic liquid: One-pot synthesis and their application," *Science of Advanced Materials* 8(5), 1135-1144. DOI: 10.1166/sam.2016.2711
- Rodrigues, F. H., Magalhães, C. E. d. C., Medina, A. L., and Fajardo, A. R. (2019). "Hydrogel composites containing nanocellulose as adsorbents for aqueous removal of heavy metals: Design, optimization, and application," *Cellulose* 26(17), 9119-9133. DOI: 10.1007/s10570-019-02736-y
- Sharma, P. R., Sharma, S. K., Lindström, T., and Hsiao, B. S. (2020). "Nanocellulose-enabled membranes for water purification: Perspectives," *Advanced Sustainable Systems* 4(5), article ID 1900114. DOI: 10.1002/advsu.201900114
- Varghese, A. G., Paul, S. A., and Latha, M. (2019). "Remediation of heavy metals and dyes from wastewater using cellulose-based adsorbents," *Environmental Chemistry Letters* 17(2), 867-877. DOI: 10.1007/s10311-018-00843-z
- Wang, S., Lu, A., and Zhang, L. (2016). "Recent advances in regenerated cellulose materials," *Progress in Polymer Science* 53, 169-206. DOI: 10.1016/j.progpolymsci.2015.07.003
- Wang, Q., Liu, S., Liu, J., Sun, J., Zhang, Z., and Zhu, Q. (2022a). "Sustainable cellulose nanomaterials for environmental remediation - achieving clean air, water, and energy: A review," *Carbohydr Polymers* 285, article ID 119251. DOI: 10.1016/j.carbpol.2022.119251
- Wang, Q., Zhou, R., Liu, S., Sethupathy, S., Liu, J., Sun, J., Zou, L., and Zhu, Q. (2022b). "Templated synthesis and assembly with sustainable cellulose nanomaterial for functional nanostructure," *Cellulose* 29(8), 4287-4321. DOI: 10.1007/s10570-022-04577-8
- Zhu, Q., Liu, S., Sun, J., Liu, J., Kirubakaran, C. J., Chen, H., Xu, W., and Wang, Q. (2020a). "Stimuli-responsive cellulose nanomaterials for smart applications," *Carbohydr Polymers* 235, article ID 115933. DOI: 10.1016/j.carbpol.2020.115933
- Zhu, Q., Yao, Q., Liu, J., Sun, J., and Wang, Q. (2020b). "Emissions from the fused filament fabrication 3d printing with lignocellulose/polylactic acid filament," *BioResources* 15(4), 7560-7572. DOI: 10.15376/biores.15.4.7560-7572
- Zhu, Q., Yao, Q., Sun, J., Chen, H., Xu, W., Liu, J., and Wang, Q. (2020c). "Stimuli induced cellulose nanomaterials alignment and its emerging applications: A review," *Carbohydr Polymers* 230, article ID 115609. DOI: 10.1016/j.carbpol.2019.115609
- Zhu, Q., Wang, J., Sun, J., and Wang, Q. (2020d). "Preparation, characterization, and oxygen barrier properties of regenerated cellulose/polyvinyl alcohol blend films," *BioResources* 15(2), 2735-2746. DOI: 10.15376/biores.15.2.2735-2746

Article submitted: June 6, 2022; Peer review completed: August 28, 2022; Revised version received and accepted: September 6, 2022; Published: September 12, 2022. DOI: 10.15376/biores.17.4.6056-6066